A Mathematically Derived Multiscale Turbulence Closure

By XIN HU[1], THOMAS Y. HOU[1] AND FAZLE HUSSAIN[2]

[1]Applied and Computational Mathematics, California Institute of Technology, Pasadena, CA91125, USA

[2]Department of Mechanical Engineering, University of Houston, Houston, TX 77204, USA

(Received ?? and in revised form ??)

Turbulence modeling is of significant importance not only for engineering applications but also for theoretical understanding. We present mathematical derivation of a closure relating the Reynolds stress to the mean strain rate for incompressible turbulent flows, without any physical assumptions. This first derivation is based on a systematic multiscale analysis, which expresses the Reynolds stress in terms of the solutions of local periodic cell problems. We reveal an asymptotic structure of the Reynolds stress by invoking the frame invariant property of the cell problems and an iterative homogenization of large and small scale solutions dynamically. We would like to point out that we don't have the closure problem encountered by other turbulent models, such as the turbulent-kinetic-energy model, and k-ε model, etc. , where intrinsic assumptions and/or empirical functions are indispensable.

In principle, this procedure of derivation could be applied to any flow in the domain with arbitrary geometry. However, in order to obtain and simplify the explicit form of the multiscale model, we need to know the characteristics of the flow. A reparameterization of the velocity in a two-scale form based on Fourier expansion is needed in order to determine the coefficient(s) in the multiscale model. The recovery of Smagorinsky model for homogeneous turbulence is presented as an example of this procedure of mathematical derivation. Another example of turbulent channel flow is given, where the modified Smagorinsky model could be simplified as the structure of flow is known. Numerical simulation results (at two Reynolds numbers) using this simplified Smagorinsky model are in good agreement with both experiments and Direct Numerical Simulations in terms of turbulent statistical quantities, such as the mean velocity profile, r.m.s. velocity and vorticity, the budget of turbulent kinetic energy, etc. in turbulent channel flow.

Key Words: Multiscale analysis, Turbulence modeling, Smagorinsky model, homogeneous turbulence, turbulent channel flow

1. Introduction

Turbulent flows can be seen everywhere in our daily life, whether it's tortuous smoke of cigars, or rip current of waterfalls, and turbulence has been a central research area in fluid dynamics since the 19th century. Navier-Stokes equations, one of the seven millennium prize problems established by the Clay Mathematics Institute, are good description of turbulent flows, according to extensive theoretical and experimental works. However, no theoretical results show that it has a (unique) solution in three dimensional space. In addition, it is extremely difficult to solve the Navier-Stokes equation because of its non-local non-linear nature.

Nowadays, thanks to the enormous progress of computer technology, it's possible to perform direct numerical simulation (DNS) of the Navier-Stokes equations. But still it requires tremendous computing resource to perform DNS of turbulent flows, especially for flows with high Reynolds number and/or irregular geometry. Many turbulent models have been established, aiming at capturing the most important statistical quantities of turbulent flows, such as the mean velocity profile, the mean kinetic energy distribution, etc. . Among them, the eddy-viscosity and mixing length model is the first attempt. But it over-simplifies the turbulent structures without considering the essential physical mechanism. Another popular model is the Smagorinsky model (see Smagorinsky 1963) and its variants(see van Driest 1956, for an example of channel flow), which have succeeded in many applications, e.g. homogeneous turbulence and turbulent channel flows.

Large eddy simulation (LES) has been able to calculate practical engineering flows in relative complex geometries (Ferziger 1977; Lesieur & Méais 1996; Rogallo & Moin 1984; Sagaut 2001). However, it is still impossible to simulate the wall-bounded flows at very high Reynolds numbers, since huge number of grid points are needed to resolve the small structure near the wall (Chapman 1979; Spalart *et al.* 1997). Recently, hybrid models, which combine LES with Reynolds Averaged Navier Stokes (RANS) equations, have been proposed to improve the modeling performance of wall-bounded turbulence (Baggett 1998; Hamba 2003). Most popular RANS models appear to yield good predictions of high Reynolds number turbulent flows. Hence, the RANS model is applied near the wall, while LES is carried out away from the wall. Spalart *et al.* (1997) proposed the detached eddy simulation (DES) by modifying Spalart-Allmaras one-equation model. The RANS simulation in the near-wall region is switched to the LES in the outer region, when the model length scale is changed from the wall distance to pseudo-Kolmogorov length scale. DES has been applied to prediction of the separated flow around a rounded-corner square at 10 deg angle of attack (Squires *et al.* 2005). Nevertheless, all these models have a closure problem, which means that these models are based on speculating some empirical formulations and/or making empirical fittings to the experimental data. No systematic mathematical derivation of such a turbulence model has been provided and validated yet.

In this paper, we present mathematical derivation based on systematic multiscale analysis of Navier-Stokes equations developed by Hou-Yang-Ran (hereafter referred to HYR, see Hou *et al.* 2005, 2008), aiming to provide an explicitly systematic derivation of the Reynolds stress term in the turbulent models. This multiscale analysis is developed in 3D homogeneous incompressible Euler and Navier-Stokes equations using a semi-Lagrangian point of view. A multiscale model can be obtained by separating variables into large scale component and small scale counterpart and considering the interactions between these two components. This gives rise to a system of coupled equations for large and small scale variables. An important feature of the multiscale formulation is that no closure assumption is required and no unknown parameters need to be determined. Therefore, it provides a self-consistent multiscale system, which captures the dynamic interaction between the large-scale velocities and the small-scale velocities. This multiscale technique has been successfully applied to 3D incompressible Navier-Stokes equations with multiscale initial data (see Hou *et al.* 2008). The multiscale analysis couples the large scale solution to a subgrid cell problem. The computational cost for this coupled system of equations is still quite expensive although an adaptive scheme has been developed to speed up the computation.

In the multiscale model, the Reynolds stress term is expressed as the average of tensor product of the small scale velocities. These small scale velocities are the solutions of a local periodic cell problem. By using the frame invariance property of the cell problem

and an iterative homogenization of large and small scale solutions dynamically, we reveal a crucial structure of the Reynolds stress. This special structure enables us to obtain an explicit form of Reynolds stress in turbulent flows without any physical assumption or empirical function. To the best of our knowledge, this is the first time that a linear constitutive relation between the Reynolds stress and the strain rate is established by combining systematic mathematical derivation and physical arguments. In principle, this procedure of mathematical derivation could be applied to any turbulent flows in the domain with arbitrary geometry, as along as the flow keeps the same features in that domain.

The paper is organized as follows: In section 2, we briefly review the multiscale analysis for the 3D Navier-Stokes equations. The systematic mathematical derivation of turbulent models, in general, based on the multiscale analysis is presented in section 3. In section 4, Smagorinsky model for homogeneous turbulence is recovered via this mathematical derivation. A simplified Smagorinsky model is obtained for turbulent channel flow and the coefficients in the model are determined and validated. Section 5 is devoted to numerical simulation and extensive comparison among the simplified Smagorinsky model, DNS and experiments. Final conclusions and remarks are presented in section 6.

2. Multiscale analysis for the 3D Navier-Stokes equations

First we review the multiscale analysis for the Navier-Stokes equations. Based on the multiscale analysis in Hou *et al.* (2005, 2008), we can formally formulate a multiscale system for the incompressible 3D Navier-Stokes equation as a homogenization problem with ϵ being a reference wave length as follows:

$$\partial_t \boldsymbol{u}^\epsilon + (\boldsymbol{u}^\epsilon \cdot \nabla)\boldsymbol{u}^\epsilon + \nabla p^\epsilon = \nu \Delta \boldsymbol{u}^\epsilon \tag{2.1a}$$

$$\nabla \cdot \boldsymbol{u}^\epsilon = 0, \tag{2.1b}$$

$$\boldsymbol{u}^\epsilon|_{t=0} = \boldsymbol{U}(\boldsymbol{x}) + \boldsymbol{W}(\boldsymbol{x}, \boldsymbol{z}), \tag{2.1c}$$

where $\boldsymbol{u}^\epsilon(\boldsymbol{x}, t)$ and $p^\epsilon(\boldsymbol{x}, t)$ are the velocity field and the pressure, respectively. The initial velocity field $\boldsymbol{u}^\epsilon(\boldsymbol{x}, 0)$ can be reparameterized in a formal two-scale structure and is separated into mean part $\boldsymbol{U}(\boldsymbol{x})$ and the high frequency component $\boldsymbol{W}(\boldsymbol{x}, \boldsymbol{z})$. In general, $\boldsymbol{W}(\boldsymbol{x}, \boldsymbol{z})$ is periodic in $\boldsymbol{z}$ with mean zero, i.e.,

$$\langle \boldsymbol{W} \rangle \equiv \int \boldsymbol{W}(\boldsymbol{x}, \boldsymbol{z})\, d\boldsymbol{z} = \boldsymbol{0}.$$

In appendix A , the reparameterization technique of the initial velocity $\boldsymbol{u}^\epsilon(\boldsymbol{x}, 0)$ in two-scale structure for turbulent channel flow is illustrated in detail. Here, the mean component $\boldsymbol{U}(\boldsymbol{x})$ and high frequency component $\boldsymbol{W}(\boldsymbol{x}, \boldsymbol{z})$ depend on the reference scale ϵ. If we take the limit $\epsilon \to 0$, $\boldsymbol{W}(\boldsymbol{x}, \boldsymbol{z})$ will tend to zero, and the mean velocity $\boldsymbol{U}(\boldsymbol{x})$ will recover the full velocity field, which contains all of the scales.

In the analysis of the structure of the multiscale solution for Euler and Naver-Stokes equations, the key idea is to use a nested multiscale expansion to characterize the propagation of small scale or high frequency component $\boldsymbol{W}(\boldsymbol{x}, \boldsymbol{z})$. The first study of homogenization theory of the 3D Euler equations with highly oscillating data was carried out by McLaughlin *et al.* (1985). To construct a multiscale expansion for the Euler equations, they made an important assumption that the oscillation is convected by the mean flow. However, Hou *et al.* performed a detailed study by using the vorticity-stream function formulation (see Hou *et al.* 2005, 2008), and they found that the small scale information is in fact propagated by the full velocity $\boldsymbol{u}^\epsilon$. To be specific, define a multiscale phase

function $\boldsymbol{\theta}^\epsilon(t,\boldsymbol{x})$ as follows:

$$\frac{\partial \boldsymbol{\theta}^\epsilon}{\partial t} + (\boldsymbol{u}^\epsilon \cdot \nabla)\boldsymbol{\theta}^\epsilon = \mathbf{0}, \tag{2.2a}$$

$$\boldsymbol{\theta}^\epsilon|_{t=0} = \boldsymbol{x}, \tag{2.2b}$$

which is also called the inverse flow map. By using this multiscale phase function, we can characterize the evolution of the small scale velocity field.

Based on a careful multiscale analysis in the Lagrangian coordinate, we obtain the following nested multiscale expansions for $\boldsymbol{\theta}^\epsilon$:

$$\boldsymbol{\theta}^\epsilon = \bar{\boldsymbol{\theta}}(t,\boldsymbol{x},\tau) + \epsilon\tilde{\boldsymbol{\theta}}(t,\bar{\boldsymbol{\theta}},\tau,\boldsymbol{\theta}^\epsilon/\epsilon), \tag{2.3}$$

where $\tau = t/\epsilon$. By making change of variables to simplify the computation of the cell problem, we perform multiscale expansion for $(\boldsymbol{u}^\epsilon, p^\epsilon)$ in the form:

$$\boldsymbol{u}^\epsilon = \bar{\boldsymbol{u}}(t,\boldsymbol{x},\tau) + \tilde{\boldsymbol{u}}(t,\bar{\boldsymbol{\theta}},\tau,\boldsymbol{z}), \tag{2.4a}$$

$$p^\epsilon = \bar{p}(t,\boldsymbol{x},\tau) + \tilde{p}(t,\bar{\boldsymbol{\theta}},\tau,\boldsymbol{z}), \tag{2.4b}$$

where $t = \tau/\epsilon$, $\boldsymbol{z} = \bar{\boldsymbol{\theta}}/\epsilon$.

Then, substituting the expansions (2.4) to the Navier-Stokes system (2.1) and averaging with respect to $\boldsymbol{z}$, we obtain the averaged equations for the mean velocity field $\boldsymbol{u}(t,\boldsymbol{x},\tau)$ with initial and proper boundary conditions:

$$\bar{\partial}_t\bar{\boldsymbol{u}} + (\bar{\boldsymbol{u}}\cdot\nabla_{\boldsymbol{x}})\bar{\boldsymbol{u}} + \nabla_{\boldsymbol{x}}\bar{p} + \nabla_{\boldsymbol{x}}\cdot\langle\tilde{\boldsymbol{u}}\otimes\tilde{\boldsymbol{u}}\rangle = \nu\nabla^2_{\boldsymbol{x}}\bar{\boldsymbol{u}} \tag{2.5a}$$

$$\nabla_{\boldsymbol{x}}\cdot\bar{\boldsymbol{u}} = 0, \tag{2.5b}$$

$$\bar{\boldsymbol{u}}|_{t=0} = \boldsymbol{U}(\boldsymbol{x}), \tag{2.5c}$$

where $\bar{\partial}_t = \partial_t + \epsilon^{-1}\partial_\tau$. The additional term $\langle\tilde{\boldsymbol{u}}\otimes\tilde{\boldsymbol{u}}\rangle$ in the averaged equation (2.5a) is the well-known Reynolds stress. How to model the Reynolds stress term is of importance in both theoretical understanding and engineering application for turbulent flows. In many LES models, the Reynolds stress is modeled by making some closure assumptions with unknown parameters to be determined by using empirical assumptions and/or fitting experimental data. In contrast, by using the frame invariance property of the cell problem and an iterative homogenization of large and small scale solutions dynamically, we reveal a crucial structure of the Reynolds stress. Then the linear constitutive relation between the Reynolds stress and strain rate can be obtained mathematically, up to second order accuracy in the time step Δt, see section 3 for more details.

Next, substituting the expansion (2.3) into (2.2) and averaging over $\boldsymbol{z}$ give us the averaged equations for $\bar{\boldsymbol{\theta}}(t,\boldsymbol{x},\tau)$ with initial and proper boundary conditions:

$$\bar{\partial}_t\bar{\boldsymbol{\theta}} + (\bar{\boldsymbol{u}}\cdot\nabla_{\boldsymbol{x}})\bar{\boldsymbol{\theta}} + \epsilon\nabla_{\boldsymbol{x}}\cdot\langle\tilde{\boldsymbol{\theta}}\otimes\tilde{\boldsymbol{u}}\rangle = \mathbf{0}, \tag{2.6a}$$

$$\bar{\boldsymbol{\theta}}|_{t=0} = \boldsymbol{x}. \tag{2.6b}$$

To simplify the model further, we only consider the leading order terms of large scale variables $(\bar{\boldsymbol{u}},\bar{p},\bar{\boldsymbol{\theta}})$

$$\bar{\boldsymbol{u}}(t,\boldsymbol{x},\tau) = \boldsymbol{u}(t,\boldsymbol{x}) + \epsilon\boldsymbol{u}_1(t,\boldsymbol{x},\tau), \tag{2.7a}$$

$$\bar{p}(t,\boldsymbol{x},\tau) = p(t,\boldsymbol{x}) + \epsilon p_1(t,\boldsymbol{x},\tau), \tag{2.7b}$$

$$\bar{\boldsymbol{\theta}}(t,\boldsymbol{x},\tau) = \boldsymbol{\theta}(t,\boldsymbol{x}) + \epsilon\boldsymbol{\theta}_1(t,\boldsymbol{x},\tau), \tag{2.7c}$$

and small scale variables $(\tilde{\boldsymbol{u}}, \tilde{p}, \tilde{\boldsymbol{\theta}})$

$$\tilde{\boldsymbol{u}} = \boldsymbol{w}(t, \bar{\boldsymbol{\theta}}, \tau, \boldsymbol{z}) + O(\epsilon), \tag{2.8a}$$
$$\tilde{p} = q(t, \bar{\boldsymbol{\theta}}, \tau, \boldsymbol{z}) + O(\epsilon), \tag{2.8b}$$
$$\tilde{\boldsymbol{\theta}} = \boldsymbol{\Theta}(t, \bar{\boldsymbol{\theta}}, \tau, \boldsymbol{z}) + O(\epsilon). \tag{2.8c}$$

This gives us simplified averaged equations, up to first order of ϵ,

$$\partial_t \boldsymbol{u} + (\boldsymbol{u} \cdot \nabla_{\boldsymbol{x}})\boldsymbol{u} + \nabla_{\boldsymbol{x}} p + \nabla_{\boldsymbol{x}} \cdot \langle \boldsymbol{w} \otimes \boldsymbol{w} \rangle = \nu \nabla_{\boldsymbol{x}}^2 \boldsymbol{u} \tag{2.9a}$$
$$\nabla_{\boldsymbol{x}} \cdot \boldsymbol{u} = 0, \tag{2.9b}$$
$$\boldsymbol{u}|_{t=0} = \boldsymbol{U}(\boldsymbol{x}), \tag{2.9c}$$

and

$$\partial_t \boldsymbol{\theta} + (\boldsymbol{u} \cdot \nabla_{\boldsymbol{x}})\boldsymbol{\theta} = \boldsymbol{0}, \tag{2.10a}$$
$$\boldsymbol{\theta}|_{t=0} = \boldsymbol{x}. \tag{2.10b}$$

Then we subtract the averaged equations from the Navier-Stokes equation (2.1) and the equations for the inverse flow map $\boldsymbol{\theta}^\epsilon$ (2.2). After some complicated algebraic operations, we obtain the equations for the small-scale variables, to the leading order approximation:

$$\partial_\tau \boldsymbol{w} + D_{\boldsymbol{z}} \boldsymbol{w} \mathcal{A} \boldsymbol{w} + \mathcal{A}^\mathsf{T} \nabla_{\boldsymbol{z}} q - \frac{\nu}{\epsilon} \nabla \cdot (\mathcal{A}\mathcal{A}^\mathsf{T} \nabla_{\boldsymbol{z}} \boldsymbol{w}) = \boldsymbol{0}, \tag{2.11a}$$
$$(\mathcal{A}^\mathsf{T} \nabla_{\boldsymbol{z}}) \cdot \boldsymbol{w} = \boldsymbol{0}, \tag{2.11b}$$
$$\boldsymbol{w}|_{t=0} = \boldsymbol{W}(\boldsymbol{x}, \boldsymbol{z}), \tag{2.11c}$$

and

$$\partial_\tau \boldsymbol{\Theta} + (\mathcal{I} + D_{\boldsymbol{z}} \boldsymbol{\Theta}) \mathcal{A} \boldsymbol{w} = \boldsymbol{0}, \tag{2.12a}$$
$$\boldsymbol{\Theta}|_{\tau=t=0} = \boldsymbol{0}, \tag{2.12b}$$

where $\mathcal{A}$ is the gradient of phase function $\boldsymbol{\theta}$, i.e. $\mathcal{A} = D_{\boldsymbol{x}} \boldsymbol{\theta}$, and $\mathcal{I}$ is the identity matrix.

Remark. An important feature of the above formulation, including the equations for both large-scale variables and high-frequency variables, does not need any closure assumption, thus no unknown parameters to be determined, in contrast to other models, e.g. , Smagorinsky model etc. . It provides a self-consistent system which captures the interaction between large-scale field and small-scale field. The computational cost for this coupled system of equations is still quite expensive although an adaptive scheme has been developed to speed up the computation, (see Hou *et al.* 2008, for an numerical example of homogeneous turbulent flows).

Remark. For the convenience of theoretical analysis and numerical implementation, the cell problem (2.11) can be further simplified by making a change of variables from $\boldsymbol{w}$ to $\tilde{\boldsymbol{w}}$ by letting $\tilde{\boldsymbol{w}} = \mathcal{A}\boldsymbol{w}$. The $\tilde{\boldsymbol{w}}$ satisfies the following modified cell problem:

$$\partial_\tau \tilde{\boldsymbol{w}} + (\tilde{\boldsymbol{w}} \cdot \nabla_{\boldsymbol{z}})\tilde{\boldsymbol{w}} + \mathcal{A}\mathcal{A}^\mathsf{T} \nabla_{\boldsymbol{z}} q - \frac{\nu}{\epsilon} \nabla \cdot (\mathcal{A}\mathcal{A}^\mathsf{T} \nabla_{\boldsymbol{z}} \tilde{\boldsymbol{w}}) = \boldsymbol{0}, \tag{2.13a}$$
$$\nabla_{\boldsymbol{z}} \cdot \boldsymbol{w} = \boldsymbol{0}, \tag{2.13b}$$
$$\tilde{\boldsymbol{w}}|_{t=0} = \mathcal{A}\boldsymbol{W}(\boldsymbol{x}, \boldsymbol{z}), \tag{2.13c}$$

3. Mathematical derivation of turbulent models

Considering that the model (2.9)–(2.12) needs huge computational CPU time and storage space, we would like to develop a simplified multiscale model. On one hand, the

new model has a comparable computational complexity with the other LES models. On the other hand, the new model needs as least closure assumptions as possible.

First of all, we state the Rivlin-Ericksen Theorem, which plays an essential role in the mathematical development of the turbulence models.

THEOREM 1 (RIVLIN-ERICKSEN). *A mapping $\widehat{T} : M^3_+ \to S^3$ is isotropic and material frame invariant if and only if it is of the form*

$$\widehat{T}(F) = \bar{T}(FF^T)$$

where the mapping $\bar{T} : S^3_+ \to S^3$ is of the form:

$$\bar{T}(B) = \beta_0(i_B)I + \beta_1(i_B)B + \beta_3(i_B)B^2$$

for every $B \in S^3_+$, where $\beta_0, \beta_1, \beta_2$ are real-valued functions of the three principal invariants i_B of the matrix B.

A complete proof of the Rivlin-Ericksen can be found in the book (Ciarlet 1988).

Note that the cell problem (2.13) for $\tilde{\boldsymbol{w}}$ is frame invariant, i.e. the following conditions are met:

(i) Translational invariance

$$\boldsymbol{x} = \boldsymbol{y} + \boldsymbol{Z}$$

where $\boldsymbol{Z}$ is a constant vector,

(ii) Galilean invariance

$$\boldsymbol{x} = \boldsymbol{y} + \boldsymbol{v}t,$$

where $\boldsymbol{v}$ is a constant vector,

(iii) Rotational invariance

$$\boldsymbol{x} = M\boldsymbol{y}$$

where M is a rotation matrix with

$$(M^{\mathsf{T}}M)_{i,j} = \delta_{i,j}.$$

Define $\mathcal{B} = \mathcal{A}\mathcal{A}^{\mathsf{T}}$, which is obviously symmetric. By Rivlin-Ericksen Theorem, we have the following relation in three-dimensional space:

$$\langle \tilde{\boldsymbol{w}} \otimes \tilde{\boldsymbol{w}} \rangle(\mathcal{B}) = a_0\mathcal{I} + a_1\mathcal{B} + a_2\mathcal{B}^2. \tag{3.1}$$

At this point, we only know that all these coefficients are the real-valued functions of the three principle invariants of $\mathcal{B}$. Furthermore, $\mathcal{B}$ cannot be solved explicitly in order to obtain these invariants.

However, in order to extract the structure of the Reynolds stress, we perform a local-in-time multiscale analysis to account for the interaction between large and small scales through dynamic re-initialization of the phase function. The large-scale components of the solution, $\boldsymbol{u}$ and θ, can generate small scales dynamically through convection and nonlinear interaction. In order to make sure that $\boldsymbol{u}$ contains only the large-scale components of the solution, we need to decompose the multiscale solution into the local mean and high frequency components by applying the reparameterization technique of HRY after solving the multiscale system for some characteristic time step Δt. This dynamic iterative reparameterization of the multiscale solution enables us to capture the dynamic interaction among all small scales of the solution. We call this procedure a dynamic iterative homogenization. More specifically, we solve the average equations (2.10) for inverse phase flow $\boldsymbol{\theta}$ in a local time interval $[t, t + \Delta t]$ with $\theta(t, \boldsymbol{x}) = \boldsymbol{x}$ as the initial condition.

By using the forward Euler method, we can approximate θ as follows:

$$\boldsymbol{\theta}(t+\Delta t,\boldsymbol{x}) = \boldsymbol{x} - \Delta t\boldsymbol{u}(t,\boldsymbol{x}).$$

Now it follows that the rate of deformation can be computed as $\mathcal{A} = D_{\boldsymbol{x}}\boldsymbol{\theta} = \mathcal{I} - \Delta t\nabla\boldsymbol{u} + O(\Delta t^2)$, and its inverse $\mathcal{A}^{-1} = \mathcal{I} + \Delta t\nabla\boldsymbol{u} + O(\Delta t^2)$. The above scheme is accurate up to the second order of time step Δt.

Therefore, $\mathcal{B}$ can be approximated up to second order of Δt as follows:

$$\mathcal{B} = \mathcal{A}\mathcal{A}^{\mathsf{T}} = \mathcal{I} - 2\Delta t\mathcal{D} + O(\Delta t^2), \tag{3.2}$$

where $\mathcal{D}$ is the rate of strain tensor defined as

$$\mathcal{D} = \frac{1}{2}\left(\nabla\boldsymbol{u} + \nabla\boldsymbol{u}^{\mathsf{T}}\right).$$

Then we have the approximation of $\langle\tilde{\boldsymbol{w}}\otimes\tilde{\boldsymbol{w}}\rangle$

$$\begin{aligned}\langle\tilde{\boldsymbol{w}}\otimes\tilde{\boldsymbol{w}}\rangle &= a_0\mathcal{I} + a_1\mathcal{B} + a_2\mathcal{B}\\ &= a_0\mathcal{I} + a_1(\mathcal{I} - 2\Delta t\mathcal{D} + O(\Delta t^2) + a_2(\mathcal{I} - 2\Delta t\mathcal{D} + O(\Delta t^2)^2\\ &= \alpha\mathcal{I} - \tilde{\beta}\Delta t\mathcal{D} + O(\Delta t^2),\end{aligned}$$

where the coefficients $\alpha = a_0 + a_1 + a_2$ and $\tilde{\beta} = 2(a_1 + a_2)$. Keep in mind that both of the coefficients α and $\tilde{\beta}$ are still the functions of the invariants of $\mathcal{B}$.

Finally, the Reynolds stress tensor is given by

$$\begin{aligned}\mathcal{R} &= \langle\boldsymbol{w}\otimes\boldsymbol{w}\rangle\\ &= \langle\mathcal{A}^{-1}\tilde{\boldsymbol{w}}\otimes\mathcal{A}^{-1}\tilde{\boldsymbol{w}}\rangle\\ &= \langle(\mathcal{I} + \Delta t\nabla\boldsymbol{u} + O(\Delta t^2))\tilde{\boldsymbol{w}}\otimes(\mathcal{I} + \Delta t\nabla\boldsymbol{u} + O(\Delta t^2))\tilde{\boldsymbol{w}}\rangle\\ &= \langle\tilde{\boldsymbol{w}}\otimes\tilde{\boldsymbol{w}}\rangle + \Delta t\nabla\boldsymbol{u}\langle\tilde{\boldsymbol{w}}\otimes\tilde{\boldsymbol{w}}\rangle + \Delta t\langle\tilde{\boldsymbol{w}}\otimes\tilde{\boldsymbol{w}}\rangle\nabla u^{\mathsf{T}} + O(\Delta t^2)\\ &= \alpha\mathcal{I} - \beta\Delta t\mathcal{D} + O(\Delta t^2).\end{aligned} \tag{3.3}$$

where $\mathrm{tr}(\mathcal{R}) = \alpha/3 = (a_0 + a_1 + a_2)/3$ is the SGS kinetic energy, and $\beta = -2a_0$. Both of them are also functions of the invariants of $\mathcal{B}$.

Remark. In equation (3.3), we establish a linear constitutive relation between the Reynolds stress $\mathcal{R}$ and the strain rate $\mathcal{D}$, up to second order accuracy in time step Δt. The first term $\alpha\mathcal{I}$ is not important since this can be incorporated by using a modified pressure. So the remaining essential question is how to determine the coefficient β. In order to specify the coefficient β, we need to know the detailed structure of the symmetric tensor $\mathcal{B}$.

Note that there exists a relation between $\mathcal{B}$ and $\mathcal{D}$ given in (3.2), so we can find the relation of the eigenvalues of $\mathcal{B}$ and $\mathcal{D}$ as follows. In three dimension, assume λ_i and $\tilde{\lambda}_i\,(i = 1,2,3)$ are the eigenvalues of $\mathcal{D}$ and $\mathcal{B}$ respectively, while $\psi_i\,(i = 1,2,3)$ are the corresponding eigenfunctions. Then, up to the second order of Δt, we have

$$\mathcal{B}\psi_i = (\mathcal{I} - \Delta t\mathcal{D})\psi_i = \tilde{\lambda}_i\psi_i, \quad i = 1,2,3,$$

which gives

$$\mathcal{D}\psi_i = \frac{1-\tilde{\lambda}_i}{\Delta t}\psi_i = \lambda_i\psi_i, \quad i = 1,2,3,$$

or

$$\tilde{\lambda}_i = 1 - \Delta t\lambda_i, \quad i = 1,2,3. \tag{3.4}$$

Further, in three dimensional space, the three invariants I_i, $(i = 1,2,3)$ of a matrix M

can be expressed by the three eigenvalues λ_i, $(i = 1, 2, 3)$ as follows

$$I_1 = \mathrm{tr}(M) = \sum_{i=1,2,3} \lambda_i,$$
$$I_2 = \frac{1}{2}\left((\mathrm{tr}(M))^2 - \mathrm{tr}(MM)\right) = \lambda_1\lambda_2 + \lambda_2\lambda_3 + \lambda_3\lambda_1,$$
$$I_3 = \det(M) = \prod_{i=1,2,3} \lambda_i.$$

Given the relations in (3.4), we can express the invariants of $\mathcal{B}$ by those of $\mathcal{D}$. Now, the coefficient β can be formulated approximately as a function of the three principle invariants of $\mathcal{D}$. For various flows, we can specify the characteristic structure of the rate of strain tensor $\mathcal{D}$ so that an explicit form for the coefficient β may be obtained. To validate our mathematical derivation of turbulent models, we first take homogeneous turbulent flow as an example for its simple geometry and physics. Later on, we will work on a more realistic channel flow, chosen because of its relevance to a large variety of engineering applications and its ability to provide direct insight into fundamental turbulence phenomena. These two examples are explained in section 4.

4. Examples: incompressible homogeneous turbulence and turbulent channel flow

Based on the mathematical analysis we have gained from the previous sections, we are now ready to give two examples to illustrate the procedure of deriving turbulent models of incompressible flows.

4.1. *Homogeneous incompressible turbulence*

For homogeneous turbulence, the flow is statistically invariant under translations and/or rotations of the reference frame. Therefore, all entries in strain tensor must be in the same order. Then, the full strain tensor $\mathcal{D}$ have to be considered:

$$\mathcal{D} = \begin{bmatrix} u_x & \frac{1}{2}(u_y + v_x) & \frac{1}{2}(u_z + w_x) \\ \frac{1}{2}(u_y + v_x) & v_y & \frac{1}{2}(v_z + w_y) \\ \frac{1}{2}(v_z + w_y) & \frac{1}{2}(v_z + w_y) & w_z \end{bmatrix}. \tag{4.1}$$

The first principle invariant of $\mathcal{D}$ is zero due to the incompressibility of turbulent flows, i.e.

$$I_1 = \mathrm{tr}(\mathcal{D}) = \nabla_{\boldsymbol{x}} \cdot \boldsymbol{u} = 0.$$

The other two invariants can be calculated as follows:

$$I_2 = \frac{1}{2}\left((\mathrm{tr}(\mathcal{D}))^2 - \mathrm{tr}(\mathcal{D}\mathcal{D})\right) = -\frac{1}{2}\left\|\mathcal{D}\right\|_F^2, \quad I_3 = \det(\mathcal{D}). \tag{4.2}$$

where $\|\cdot\|_F$ is the Frobeniun norm, i.e. $\|\mathcal{D}\|_F = \sqrt{\sum_i \sum_j |\mathcal{D}_{ij}|^2}$. From dimensional analysis, we find that the coefficient β has the dimension of $\|\mathcal{D}\|_F$. Thus, we assume that β is a linear function of $\|\mathcal{D}\|_F$, i.e.

$$\beta(I_1, I_2, I_3) = C_s^2 \left\|\mathcal{D}\right\|_F,$$

where C_s is a universal constant because of homogeneity. A simple scaling analysis shows the scaling relation $\Delta t \sim \Delta^2$ for the Navier-Stokes equations, where Δ is a typical length for the large-scale solutions. Finally, we recover the Smagorinsky model for homogeneous

TABLE 1. Quantitative order of the velocity derivatives.

$\partial u/\partial x$	$\partial u/\partial y$	$\partial u/\partial z$	$\partial v/\partial x$	$\partial v/\partial y$	$\partial v/\partial z$	$\partial w/\partial x$	$\partial w/\partial y$	$\partial w/\partial z$
$\sim 10^{-2}$	$\sim 10^{2}$	$\sim 10^{-2}$	$\sim 10^{-4}$	$\sim 10^{-1}$	$\sim 10^{-4}$	$\sim 10^{-2}$	$\sim 10^{2}$	$\sim 10^{-1}$

turbulence, up to second order accuracy of time step, as stated in the following

$$\mathcal{R} = -(C_s\Delta)^2 \left\|\mathcal{D}\right\|_F \mathcal{D}.$$

The constant $C_s = 0.18$, which can be estimated by using the $k^{-5/3}$ Kolmogorov cascade to make the ensemble-averaged subgrid kinetic energy dissipation identical to the kinetic energy (Lilly 1987).

4.2. *Turbulent channel flow*

The argument for homogeneous turbulence also applies for turbulent channel flow and it leads to the following modified Smagorinsky model by adding the van Driest damping function

$$\mathcal{R} = -(C_m\Delta(1-\exp(y^+/A)))^2 \left\|\mathcal{D}\right\|_F \mathcal{D},$$

where y^+ is the non-dimensional distance from the wall and $A = 25$ is the van Driest constant (van Driest 1956). However, we can simplify the Smagorinsky model by taking advantage of the special structure of the strain rate $\mathcal{D}$ for turbulent channel flow. Specifically, by an asymptotic boundary layer analysis, we find the orders of the velocity derivatives as follows:

$$\frac{\partial u}{\partial y}, \frac{\partial w}{\partial y} \gg \frac{\partial u}{\partial x}, \frac{\partial u}{\partial z}, \frac{\partial v}{\partial y}, \frac{\partial w}{\partial x}, \frac{\partial w}{\partial z} \gg \frac{\partial v}{\partial x}, \frac{\partial v}{\partial z}.$$

The scaling analysis of the velocity derivatives near the wall is consistent with the numerical results obtained by Direct Numerical Simulation (DNS), see Table 1. Given the orders of the velocity derivatives, we neglect the small quantities in the entries of $\mathcal{D}$. Thus, $\mathcal{D}$ can be approximated as follows

$$\mathcal{D} \sim \begin{bmatrix} 0 & u_y/2 & 0 \\ u_y/2 & 0 & w_y/2 \\ 0 & w_y/2 & 0 \end{bmatrix}. \tag{4.3}$$

The eigenvalues of the above approximate $\mathcal{D}$ are $\lambda_1 = 0$, $\lambda_{2,3} = \pm\sqrt{u_y^2 + w_y^2}/2$. Thus it follows that the three principle invariants are $I_1 = I_3 = 0$, $I_2 = -(u_y^2 + w_y^2)/4$. Now, the coefficients α and β are functionals of I_2 or $u_y^2 + w_y^2$ only. Based on the same arguments as homogeneous turbulence, we propose the following form for β:

$$\beta = f(y)(u_y^2 + w_y^2)^{1/2},$$

where $f(y)$ is a function of y or y^+ due to the inhomogeneity in y direction. By fitting using DNS, $f(y^+)$ is found to be shaped as damping van Driest function

$$f(y^+) = C_m^2((1-\exp(y^+/A)))^2,$$

where C_m is the universal constant, y^+ is the non-dimensional distance from the wall, and $A = 25$ is the van Driest constant (van Driest 1956). The distance from the wall

measured in wall units is important in the turbulent channel flow and defined as follows

$$y^+ = \frac{u_\tau(\delta - |y|)}{\nu}, \tag{4.4}$$

where δ is the channel half-width, u_τ is the wall shear velocity, and ν is the viscosity.

Finally, based on the multiscale analysis, we propose a simplified model for the Reynolds stress

$$\mathcal{R} = -(C_m\Delta(1-\exp(y^+/A)))^2(u_y^2+w_y^2)^{1/2}\mathcal{D}. \tag{4.5}$$

Remark. In the simplified model (4.5), Reynolds stress reduces to 0 naturally as the boundary is approached due to van Driest damping function (see van Driest 1956; Pope 2000; Berselli *et al.* 2006). This property ensures that the non-slip boundary condition on walls is preserved.

The constant C_m can be determined by locally minimizing the Reynolds stress error term

$$\min_{C_m} \left\| R - \alpha\mathcal{I} + \left(C_m\Delta(1-\exp(y^+/A))(u_y^2+w_y^2)^{1/4}\right)^2 \mathcal{D} \right\|_F.$$

This gives us

$$C_m = \frac{\sqrt{-\mathcal{R}_d : \mathcal{D}}}{\Delta(1-\exp(y^+/A))(u_y^2+w_y^2)^{1/4}\left\|\mathcal{D}\right\|_F}, \tag{4.6}$$

where $\mathcal{R}_d = \mathcal{R} - \mathrm{tr}(\mathcal{R})\mathcal{I}/3$ and $\mathcal{R}_d : \mathcal{D} = \sum_{i,j}(\mathcal{R}_d)_{ij}\mathcal{D}_{ij}$. We perform *a priori* calculation to calculate $\mathcal{R}_d$ in equation (4.6) using the multiscale formulation elaborated in the following algorithm.

Algorithm 1 (Determining the constant C_m).

(i) Run a DNS simulation of (2.1) *to get the full velocity field* $\boldsymbol{u}^\epsilon(\boldsymbol{x}_i, t_n)$ *at each time step,*

(ii) Perform a reparameterization procedure, which is based on the Fourier expansion and explained in detail in Appendix A for the channel flow, to obtain $\boldsymbol{u}(\boldsymbol{x}_i, t_n)$ *and* $\boldsymbol{w}(\boldsymbol{x}_i, t_n, \boldsymbol{x}_i/\epsilon, t_n/\epsilon)$,

(iii) The reynolds stress is given by

$$\mathcal{R}(\boldsymbol{x}, t) = \langle \boldsymbol{w} \otimes \boldsymbol{w} \rangle. \tag{4.7}$$

4.3. *Verification of the Algorithm 1 and determination of constant* C_m

In order to validate the algorithm 1, we run a test on a classical eddy viscosity model, the Smagorinsky model with van Driest damping . The Smagorinsky model (Smagorinsky 1963) can be derived from the $k^{-5/3}$ spectra theorem. For the channel flow, boundary layer in the normal direction introduces a large amount of dissipation. The extra dissipation prevents the formation of the eddies, thus eliminating turbulence from the beginning. Therefore, the van Driest damping is introduced to reduce the Smagorinsky constant C_S to 0 when approaching the walls (for more discussions, see Pope 2000; Sagaut 2001). The Smagorinsky model with van Driest damping for Reynolds stress reads as

$$\mathcal{R}(\boldsymbol{x}, t) = -(C_s\Delta(1-\exp(y^+/A)))^2 \left\|\mathcal{D}\right\|_F \mathcal{D}, \tag{4.8}$$

where C_s is the Smagorinsky constant, $\Delta = \sqrt[3]{\Delta_x\Delta_y(y)\Delta_z}$ is the filter width, y^+ is the non-dimensional distance from the wall.

The constant C_s can be estimated by using the $k^{-5/3}$ Kolmogorov cascade to make the ensemble-averaged subgrid kinetic energy dissipation identical to ε, which is the kinetic

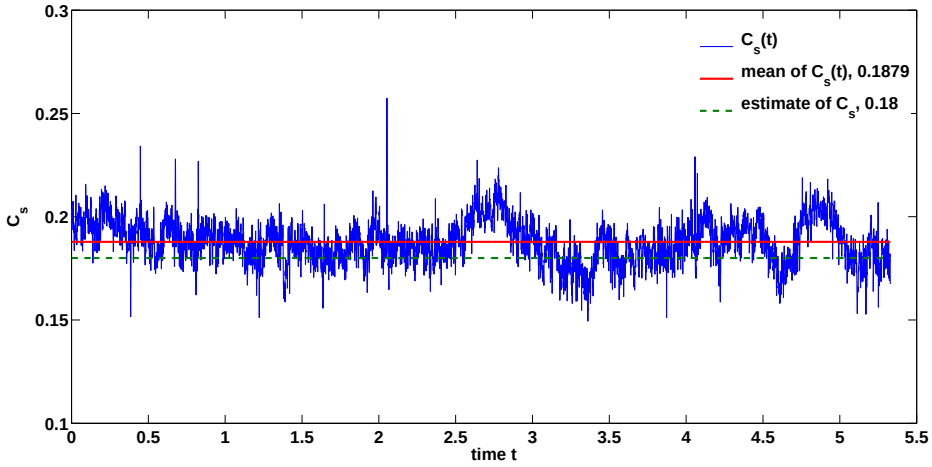

FIGURE 1. Temporal evolution of the constant C_s in the Smagorinsky model with van Driest damping function. The dashed line denotes the value of 0.18, which can be estimated by using the $k^{-5/3}$ Kolmogorov cascade to make the ensemble-averaged subgrid kinetic energy dissipation identical to the kinetic energy (Lilly 1987).

energy (see the review by Lilly 1987). An approximate value for the constant is then

$$C_s \approx \frac{1}{\pi}\left(\frac{3C_K}{2}\right)^{-3/4}. \tag{4.9}$$

For a Kolmogorov constant C_K of 1.4, which is obtained by measurements in the atmosphere (Champagne *et al.* 1977), this yields $C_s \approx 0.18$.

On the other hand, using the technique of an iterative homogenization of large and small scale solutions dynamically and locally minimizing the Reynolds stress error, the Smagorinsky constant C_s can be determined as follows:

$$C_s = \frac{\sqrt{-\mathcal{R}_d : \mathcal{D}}}{\Delta(1-\exp(y^+/A))\,\|\mathcal{D}\|_F\,\sqrt{\|\mathcal{D}\|_F}}. \tag{4.10}$$

In figure 1, we plot the evolution of the Smagorinsky constant C_s. It can be seen that the Smagorinsky constant C_s oscillates slightly around the value of 0.18, showing that algorithm 1 determines the Smagorinsky constant accurately. Figure 2 indicates that the constant C_m varies around 0.2074. This is the value we will take for C_m in the following numerical simulation with the simplified Smagorinsky model for turbulent channel flow.

5. Turbulent channel flow: numerical results and discussions

In this section, we present an extensive numerical study of the simplified Smagorinsky model (4.5). The turbulent statistical quantities obtained by the simplified model are compared comprehensively with both experimental and DNS results for two Reynolds numbers $Re_\tau = 180$ and $Re_\tau = 395$.

5.1. *Numerical Methods and Settings.*

In order to examine the structure of the rate of strain tensor $\mathcal{D}$, we need to perform a DNS run. We use the same computational domain as that in Kim *et al.* (1987), see figure

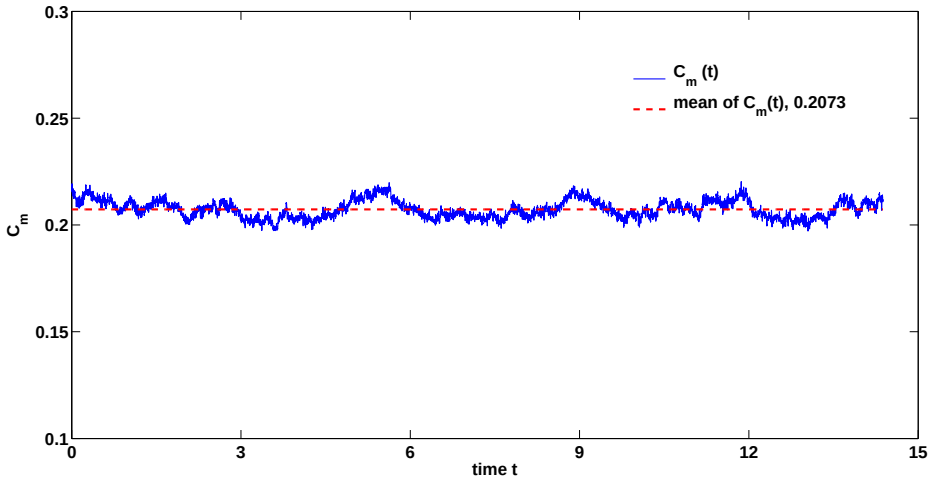

FIGURE 2. Temporal evolution of the constant C_m in the simplified Smagorinsky model obtained by Algorithm 1. The dashed line denotes the value of 0.2073, which is a universal constant for the turbulent channel flow.

3. The streamwise (x) and spanwise (z) computational periods are chosen to be 4π and 2π, and the half-width of the channel is 1. Fully developed turbulent flow in a channel is homogeneous in the streamwise and spanwise directions. Therefore, we assume periodic boundary conditions in these two directions. The no-slip boundary condition is chosen in the wall-normal direction (y).

The numerical scheme uses a Chebychev-tau formulation in the wall-normal direction (y) and Fourier expansions in the streamwise (x) and spanwise (z) directions. Further, we make a change of variables in the Chebyshev expansion to take advantage of the Fourier transform. In DNS by Kim *et al.* (1987), the 2/3 rule was used to remove the aliasing errors induced by the pseudo-spectral method. Here, we use the high order Fourier smoothing method introduced by Hou & Li (2007). A low-storage third order Runga-Kutta time discretization developed by Spalart *et al.* (1994) is used. A constant pressure gradient is applied to drive the flow in the streamwise direction. For DNS with $Re_\tau = 180$, Kim *et al.* (1987) used an effective resolution $128(x) \times 129(y) \times 128(z)$, while we use only $64(x) \times 65(y) \times 64(z)$ for the simplified Smagorinsky model. For DNS with $Re_\tau = 395$, Moser *et al.* (1999) used an effective resolution $256(x) \times 257(y) \times 256(z)$. In comparison, we use only $128(x) \times 129(y) \times 128(z)$ for the simplified model.

The fully developed turbulent flow in a channel using the simplified Smagorinsky model is obtained by taking first N modes of velocity given by the DNS as initial data, where N is the number of grid points used for the simulation of the simplified model. The code is run by integrating forward in time until a statistically steady state is achieved. The steady state is identified by quasi-periodic behavior of the total kinetic energy and by a linear profile of total shear stress, $-\overline{u'v'} + (1/Re)\partial\bar{u}/\partial y$. Once the velocity field reaches the statistically steady state, the simplified model is further integrated in time to obtain a time average of a variety of statistical variables. The statistical variables are obtained by averaging over horizontal plane (both homogeneous directions x and z) and time t. The coordinates and flow variables are normalized by the channel half width δ, the kinematic viscosity ν, and the friction velocity $u_\tau = (\tau_w/\rho)^{1/2}$, where τ_w is the statistically averaged wall shear stress and ρ is the density.

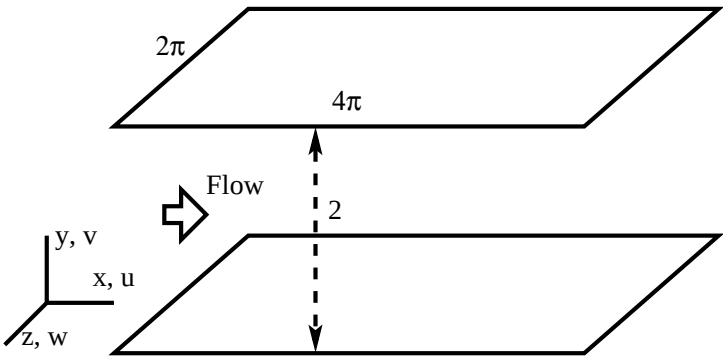

FIGURE 3. Computational domain in a channel.

5.2. *Turbulent structure near the wall*

The two most prominent structural features of the near-wall turbulence are illustrated in figures 4 and 5:

(i) Streaks of low momentum fluid, regions of $u' < 0$, which have been lifted into the buffer region by the vortices.

(ii) Elongated streamwise vortices, identified by the region of negative λ_2 proposed by Jeong & Hussain (1995).

Currently, it is well accepted that near wall streamwise vortices by Biot-Savart induction lifts the low speed fluid to form the streaks. On the other hand, the streamwise vortices are generated from the many normal-mode-stable streaks via a new scenario, identified by the streak transient growth (STG) mechanism (for details, see Schoppa & Hussain 2002). The phase averages of the vortices, their characteristics and their dynamical role have been discussed by Jeong *et al.* (1997).

5.3. *Mean flow properties*

Figure 6 shows the profile of the mean velocity normalized by the wall-shear velocity u_τ for $Re_\tau = 180$. In the viscous sublayer $y^+ < 10$, we observe excellent agreement with the linear relation $u^+ = y^+$. In the log-law region ($y^+ > 30$, $y/\delta < 0.3$), it is well known that the logarithmic law of the wall due to von Kármán (1930) can be expressed as

$$u^+ = \frac{1}{\kappa} \ln y^+ + B,$$

where $\kappa = 0.41$ is the Kármán constant and B is the additive constant. In the simplified Smagorinsky model, the additive constant B is 5.5, which is exactly the approximate value reported in the literature (Eckelmann 1974; Kim *et al.* 1987; Spalart 1988). In the log-law region, the profiles of mean streamwise velocity of both the simplified model and DNS Kim *et al.* (1987) are lower than experimental results by Eckelmann (1974).

The profile of the mean velocity u^+ for $Re_\tau = 395$ is shown in figure 7 and compared to the DNS results obtained by Moser *et al.* (1999) and the experimental results by Hussain & Reynolds (1970) for $Re_\tau = 642$. In the viscous sublayer, the results of simplified model obey the linear relation accurately. The profile conforms to the log law with the constant $B = 5.5$ in the log-law region, while both DNS by Moser *et al.* (1999) and our simplified model give slightly larger values of u^+ than the experiments by Hussain & Reynolds (1970).

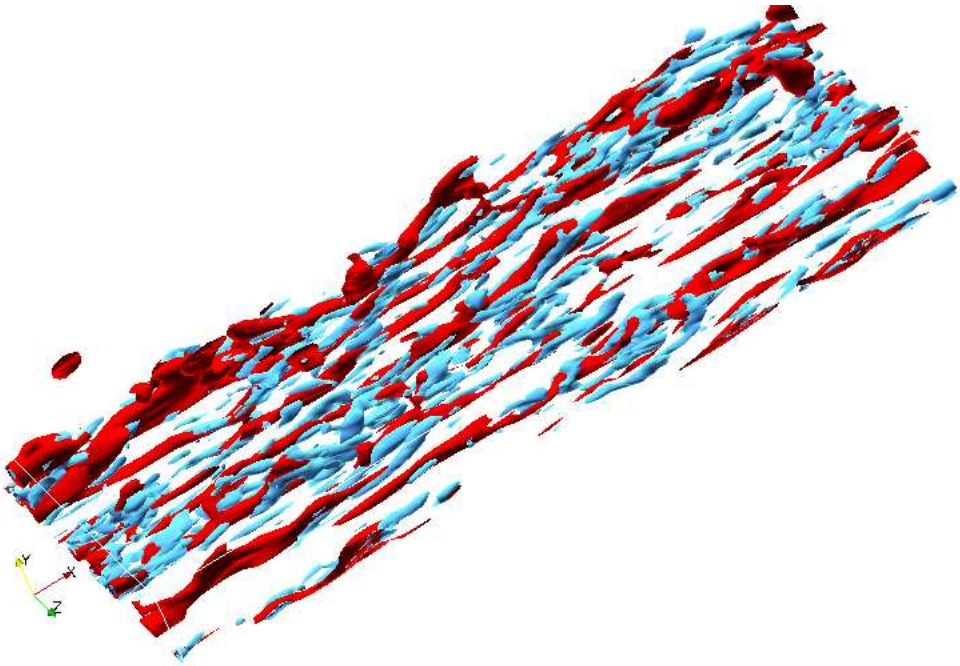

FIGURE 4. Turbulent structure near the wall obtained using simplified Smagorinsky model; Iso-surface of streamwise vortices (blue) indicated by the $\lambda_2 < 0$ vortex definition (Jeong & Hussain 1995) and lifted low-speed streaks (red) denote $u' < 0$ in the region $0 < y^+ < 60$, $Re_\tau = 180$.

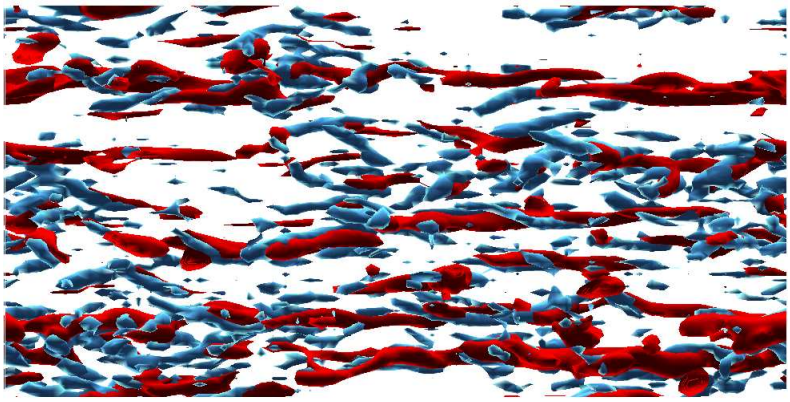

FIGURE 5. Top view of turbulent structure near the wall; Iso-surface of streamwise vortices (blue) indicated by the $\lambda_2 < 0$ vortex definition (Jeong & Hussain 1995) and lifted low-speed streaks (red) denote $u' < 0$ in the region $0 < y^+ < 60$, $Re_\tau = 180$.

5.4. *Turbulence intensities*

One of the Reynolds number effects in wall-bounded turbulence is in the root-mean-square (r.m.s.) velocity profiles (u', v', w'). These turbulence intensities normalized by the wall-shear velocity are shown and compared with DNS (Kim *et al.* 1987; Moser *et al.* 1999) and experiments (Kreplin & Eckelmann 1979) in figure 8 for $Re_\tau = 180$ and figure 9 for $Re_\tau = 395$, respectively, whenever the data are available.

In the case of $Re_\tau = 180$, the profiles obtained by the simplified model are in good

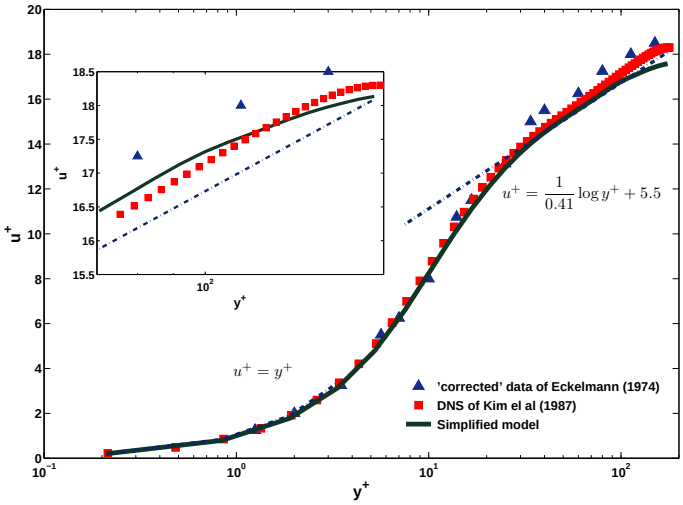

FIGURE 6. Near wall profiles of mean streamwise velocity u^+ for $Re_\tau = 180$, compared with DNS by Kim *et al.* (1987) and experiments by Eckelmann (1974).

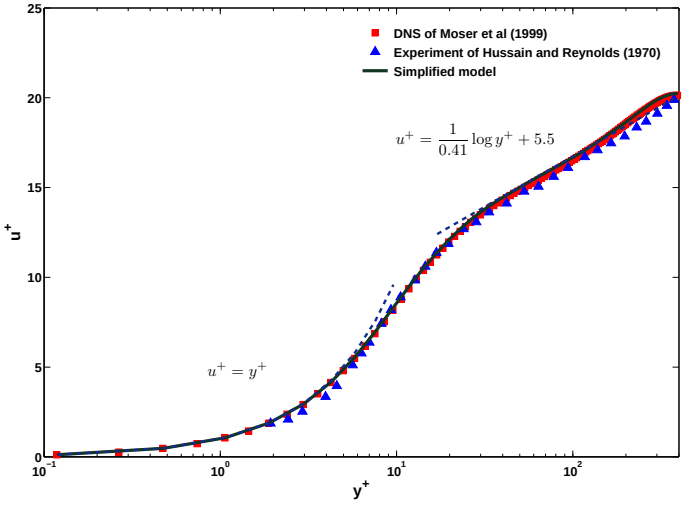

FIGURE 7. Near wall profiles of mean streamwise velocity u^+ for $Re_\tau = 395$, compared with DNS by Moser *et al.* (1999) and experiment by Hussain & Reynolds (1970).

agreement with those of Kim *et al.* (1987) and Kreplin & Eckelmann (1979), although the peak value of $u_{\rm rms}$, about 2.5, is lower. The value of $u_{\rm rms}$ obtained by DNS is slightly higher. This may be because of the high damping coefficient near the wall. As pointed out in Kim *et al.* (1987), these values of numerical simulations are lower than the measured values in the experiment by Kreplin & Eckelmann (1979). The r.m.s. spanwise velocity

[h]

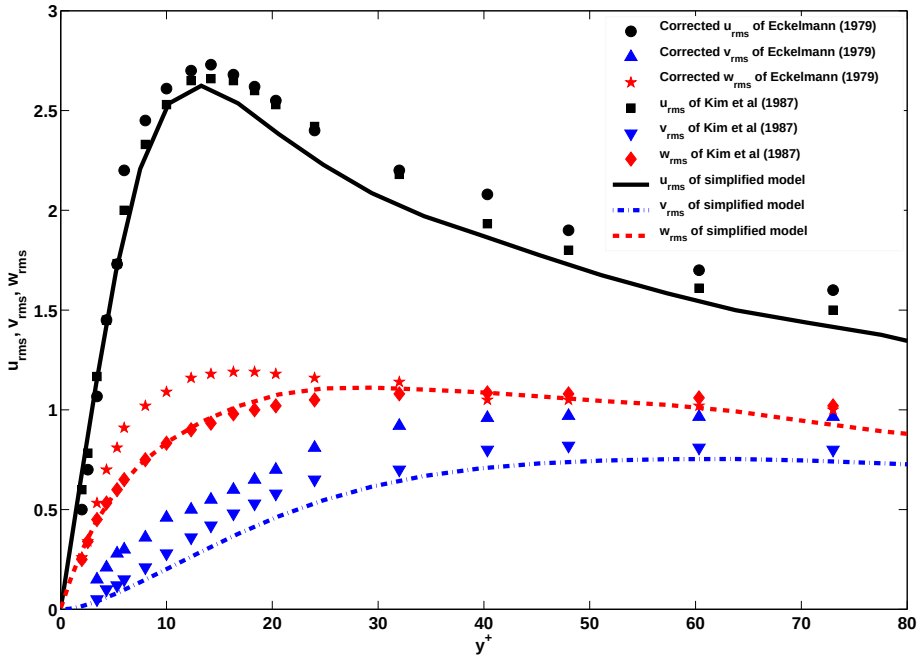

FIGURE 8. Root-mean-square velocity fluctuations normalized by the wall shear velocity u_τ by the simplified model for $Re_\tau = 180$, compared with DNS by Kim *et al.* (1987) and experiments by Kreplin & Eckelmann (1979).

fluctuation $w_{\rm rms}$ is in remarkably good agreement with Kim *et al.* (1987). But both of them are lower than the experimental results (Kreplin & Eckelmann 1979) near the wall.

In the case of $Re_\tau = 395$, the peak value of $u_{\rm rms}$ is much higher than DNS results by Moser *et al.* (1999) around $y^+ = 20$. The values of $u_{\rm rms}$ and $w_{\rm rms}$ of the simplified model are higher than DNS when $y^+ < 20$. After that, the value drops faster and eventually becomes lower than DNS. On the other hand, the values of $v_{\rm rms}$ match quit well throughout computational domain between the simplified model and DNS. Moreover, as observed of Spalart (1988), the peak value of the $u_{\rm rms}$ is Reynolds number dependent, which is clearly shown by comparing $u_{\rm rms}$ in figure 8 and figure 9. Antonia *et al.* (1992) pointed out that the Reynolds number dependence for $w_{\rm rms}$ is significant compared to that for $u_{\rm rms}$ and $v_{\rm rms}$. This is also demonstrated in figure 8 and 9. In the present results of the simplified model, all three root mean square velocity fluctuations are enhanced with increasing Reynolds number. This may be because the energy redistribution increases remarkably for $u_{\rm rms}$, $v_{\rm rms}$, $w_{\rm rms}$.

Figure 10 and 11 show the profile of r.m.s. pressure normalized by the wall shear velocity and density, $p_{\rm rms}/\rho u_\tau^2$ for $Re_\tau = 180$ and $Re_\tau = 395$, respectively. For $Re_\tau = 180$, the simplified model gives a value of about 1.84 on the wall, compared to 1.5 of DNS by Kim *et al.* (1987). Moreover, it has a maximum value of about 2.2 at $y/\delta \approx \pm 0.9$. This is even better than that in DNS by Kim *et al.* (1987) when compared to

[h]

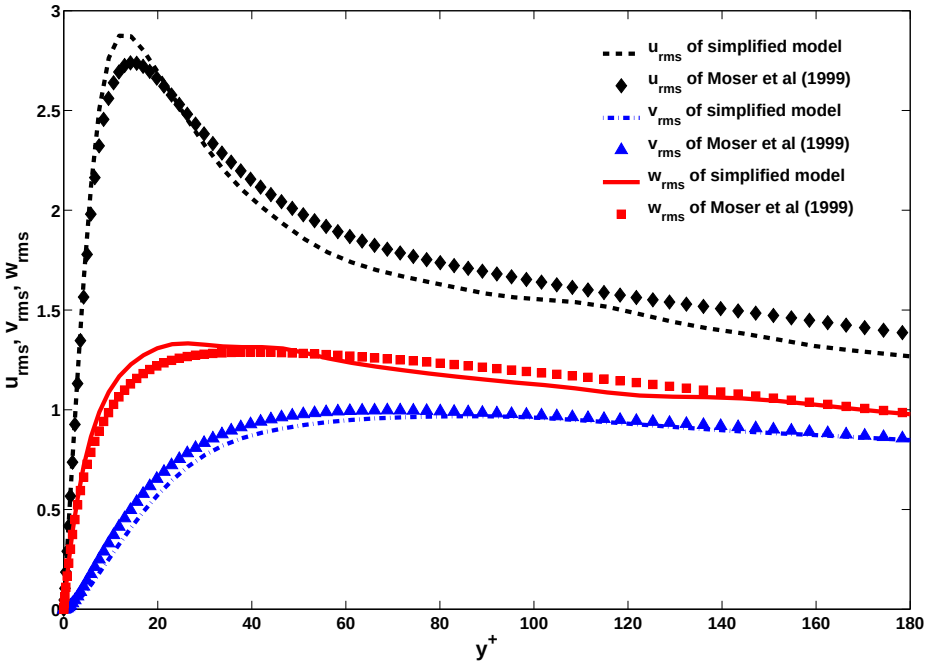

FIGURE 9. Root-mean-square velocity fluctuation normalized by the wall shear velocity u_τ by the simplified model for $Re_\tau = 395$, compared with DNS by Moser *et al.* Moser *et al.* (1999).

the experiments conducted by Willmarth (1975). The experimental results show that the r.m.s. wall pressure in a turbulent boundary layer varies between 2 and 3. This is also true for the case of $Re_\tau = 395$, in which the maximum value of r.m.s. wall pressure fluctuation is about 2.42 for the simplified model, see figure 11. Willmarth (1975) also shows a definite increasing trend of the r.m.s. wall pressure fluctuations with Reynolds number, which is demonstrated in figures 10 and 11 with two Reynolds numbers.

5.5. *Reynolds shear stress*

The total shear stress, $-\overline{u'v'} + (1/Re)\partial\bar{u}/\partial y$, is shown in figure 12 for the simplified model at two Reynolds numbers $Re_\tau = 180$ and $Re_\tau = 395$. In the fully developed turbulent channel flow considered in this section, this profile is a straight line when the flow reaches an equilibrium state. For this simplified model, figure 12 clearly shows that our computations of the two Reynolds numbers have achieved statistically steady state. The behavior of the Reynolds shear stress in the immediate vicinity of the wall can be explained by the following nondimensionalized equation (Tennekes & Lumley 1972)

$$-\frac{\overline{u'v'}}{u_\tau^2} + \frac{\mathrm{d}u^+}{\mathrm{d}y^+} = 1 - \frac{y^+}{\delta^+}, \tag{5.1}$$

where $\delta^+ = u_\tau\delta/\nu$. The stress at the wall is purely viscous. Nondimensionalized in this way, the Reynolds number dependence is absorbed in the scale for y so that the viscous term does not become small at large Reynolds numbers. Thus, for small y^+/δ^+,

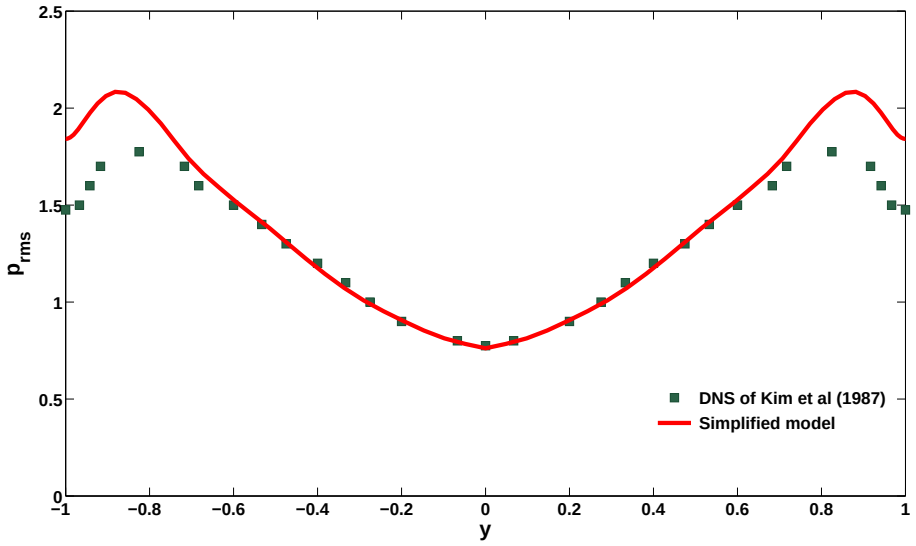

FIGURE 10. Root-mean-square pressure fluctuation normalized by the wall shear velocity and density, $p_{\rm rms}/\rho u_\tau^2$ for $Re_\tau = 180$, compared with. DNS by Kim *et al.* (1987)

the Reynolds shear stress does not vary with Reynolds numbers and collapses into one curve. In figure 12, the two lines are close to each other, especially near the wall when $|y|$ close to 1. Also, it can be seen that the slopes for $Re_\tau = 180$ and $Re_\tau = 395$ are close to 1 as well, as confirmed in (5.1).

5.6. *Vorticity*

The root mean square of vorticity fluctuations, normalized by the mean shear at the wall $\omega_i\nu/u_\tau^2, (i = x, y, z)$, are shown in figures 13 and 14 for $Re_\tau = 180$ and $Re_\tau = 395$, respectively.

The simplified model results agree very well with the DNS results Kim *et al.* (1987). On the wall, the values of $\omega_x\nu/u_\tau^2$ given by the multiscale model and DNS are larger than that obtained experimentally Kreplin & Eckelmann (1979). Away from the wall, the multiscale model performs slightly worse than DNS Kim *et al.* (1987) when compared to the limited experimental data Kastrinakis & Eckelmann (1983) in terms of $\omega_x\nu/u_\tau^2$.

Near the wall, the streamwise and spanwise vorticity fluctuations increase with increasing Reynolds number. Especially, r.m.s. ω_z shows a larger value for a higher Reynolds number.This is simply because of the large shear stress at the immediate vicinity of the wall. To see this in detail, write down the vorticity equation in the local coordinates (x, n, s) (Lamb 1945) for linearized perturbations of a $U(x)$ streak distribution, the inviscid evolution equation for vorticity perturbation ω_x', which is the most important component, can be derived as

$$\frac{\partial \omega_x'}{\partial t} + \bar{u}\frac{\partial \omega_x'}{\partial x} = h_s\Omega\frac{\partial u_x'}{\partial s} + h_n\omega_n'\frac{\mathrm{d}\bar{u}}{\mathrm{d}n} = \Omega\frac{\partial u_s'}{\partial x}, \tag{5.2}$$

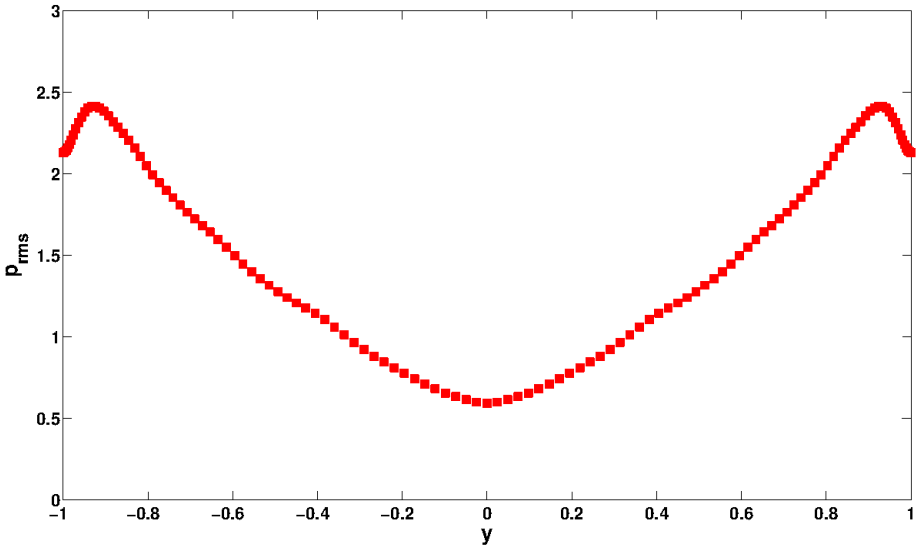

FIGURE 11. Root-mean-square pressure fluctuation normalized by the wall shear velocity and density, $p_{\rm rms}/\rho u_\tau^2$ for $Re_\tau = 395$.

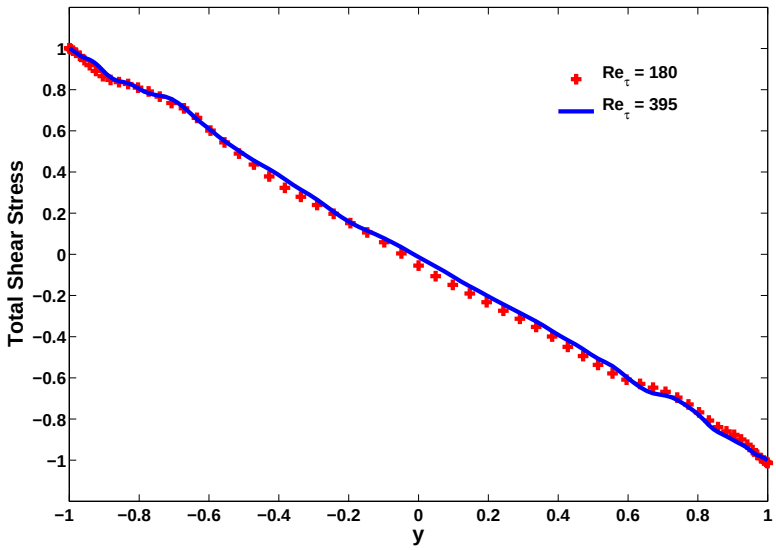

FIGURE 12. Total shear stress, $-\overline{u'v'} + (1/\mathrm{Re})\partial\bar{u}/\partial y$, normalized by the wall shear velocity for $Re_\tau = 180$ and $Re_\tau = 395$.

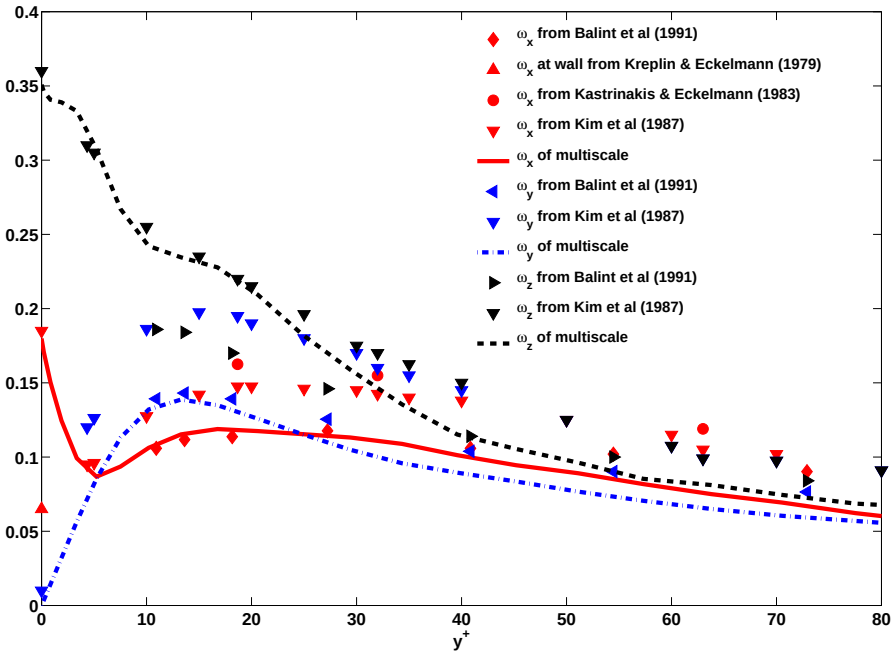

FIGURE 13. Root-mean-square vorticity fluctuations normalized by the mean shear near the wall for $Re_\tau = 180$, compared with DNS by Kim *et al.* (1987) and experiments by Kreplin & Eckelmann (1979), Kastrinakis & Eckelmann (1983) and Balint *et al.* (1991).

where the direction cosine amplitudes h_n and h_s are determined from

$$h_n^2 = \left(\frac{\partial n}{\partial y}\right)^2 + \left(\frac{\partial n}{\partial z}\right)^2, \quad h_s^2 = \left(\frac{\partial s}{\partial y}\right)^2 + \left(\frac{\partial s}{\partial z}\right)^2. \tag{5.3}$$

The base flow vorticity is given by $\Omega = -h_n \mathrm{d}\bar{u}/\mathrm{d}n$ in the local coordinates, which permits simplification by combining the two ω_x' production terms. Thus, the profile of u_s' is critical for ω_x' generation. This has been illustrated in the streak transient growth mechanism for the generation of near-wall streamwise vortices by Schoppa & Hussain (2002).

5.7. *Budget of turbulent kinetic energy k*

For fully developed turbulent channel flow, the balance equation for turbulent kinetic energy is (Pope 2000)

$$0 = \mathcal{P} - \tilde{\varepsilon} + \nu \frac{\mathrm{d}^2 k}{\mathrm{d}y} - \frac{\mathrm{d}}{\mathrm{d}y}\langle \tfrac{1}{2} v \mathbf{u}\cdot\mathbf{u}\rangle - \frac{1}{\rho}\frac{\mathrm{d}}{\mathrm{d}y}\langle v p'\rangle. \tag{5.4}$$

Budget terms of the turbulent kinetic energy in (5.4) are given by

(i) The production term

$$\mathcal{P} = -\langle u_i u_j\rangle \frac{\partial \langle U_i\rangle}{\partial y}. \tag{5.5}$$

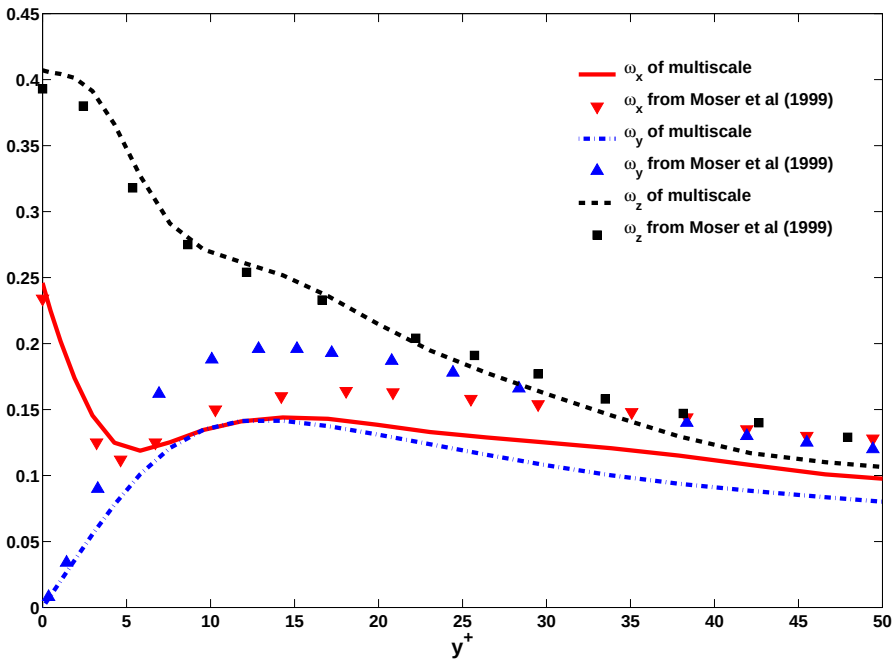

FIGURE 14. Root-mean-square vorticity fluctuations normalized by the mean shear near the all for $Re_\tau = 395$, compared with DNS by Moser *et al.* Moser *et al.* (1999).

(ii) the dissipation term

$$-\tilde{\varepsilon} = -\left(2\nu\langle s_{ij}s_{ij}\rangle - \nu\frac{\partial^2\langle u_i u_j\rangle}{\partial x_i \partial x_j}\right), \tag{5.6}$$

where s_{ij} is the fluctuating rate of strain:

$$s_{ij} = \frac{1}{2}\left(\frac{\partial u_i}{\partial x_j} + \frac{\partial u_j}{\partial x_i}\right). \tag{5.7}$$

(iii) the viscous dissipation term

$$\nu\frac{\mathrm{d}^2 k}{\mathrm{d}y}. \tag{5.8}$$

(iv) the turbulent convection term

$$-\frac{\mathrm{d}}{\mathrm{d}y}\langle\tfrac{1}{2}v\mathbf{u}\cdot\mathbf{u}\rangle. \tag{5.9}$$

(v) pressure transport

$$-\frac{1}{\rho}\frac{\mathrm{d}}{\mathrm{d}y}\langle vp'\rangle. \tag{5.10}$$

Figures 15 and 16 show the budget terms of the turbulent kinetic energy normalized by ν/u_τ^4 for Reynolds number $Re_\tau = 180$ and $Re_\tau = 395$ obtained by the simplified model. The results are compared with DNS by Kim *et al.* (1987) and Moser *et al.* (1999).

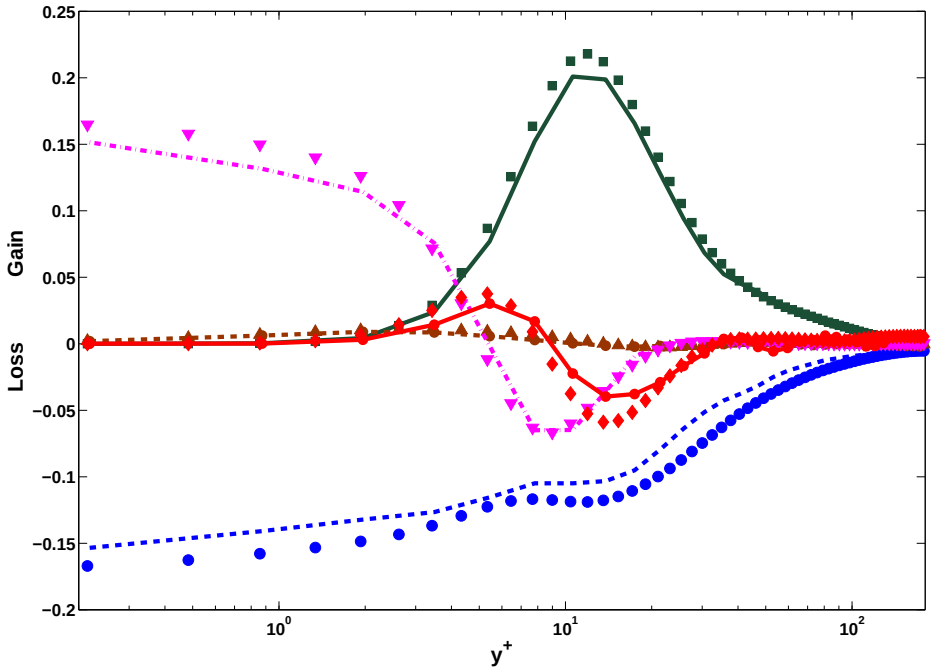

FIGURE 15. The turbulent-kinetic budget normalized by ν/u_τ^4 near the wall for $Re_\tau = 180$, compared with DNS by Kim *et al.* (1987). Production term: simplified model, solid line; DNS, square. Dissipation term: simplified model, dash-dash line; DNS, circle; Pressure transport term: simplified model, dash-dash line with circle; DNS, up-triangle. Viscous diffusion term: simplified model, dash-dot line; DNS, down-triangle. Turbulent convection term: simplified model, solid line with circle; DNS, diamond.

For $Re_\tau = 180$, each kinetic energy budget term obtained by the simplified model agrees well with DNS by Kim *et al.* (1987). More specifically, the production behaves like the order of y^3 from 0 near the wall. For the simplified model, the production reaches the peak value at around $y^+ = 12$, where the production-to-dissipation ratio is approximately 1.8, which agrees with the ratio obtained by Kim *et al.* (1987).

The effects of different Reynolds numbers on all these budget terms are reflected in the comparison of figures 15 and 16 for $Re_\tau = 180$ and $Re_\tau = 395$, respectively. The values of all terms in the budget of the turbulent kinetic energy increase with the increase of Re_τ. Especially, the wall values of the dissipation and the viscous dissipation increase remarkably with the increasing Reynolds number. This is simply because the increase of the shear stress dominates the decrease of the viscosity.

5.8. *Mixing length*

One of the most popular models for Reynolds stress in the turbulence modeling community is the mixing length model proposed by Prandtl (1925), which is based on two essential assumptions: (i) the characteristic length l_m in the approach $u' \sim l_m \frac{\mathrm{d}\bar{u}}{\mathrm{d}y}$ is proportional to the distance y from the wall; (ii) the v' fluctuations normal to the wall and the u' fluctuations in the spanwise direction behave similarly, i.e. $v' \sim u'$. This approach

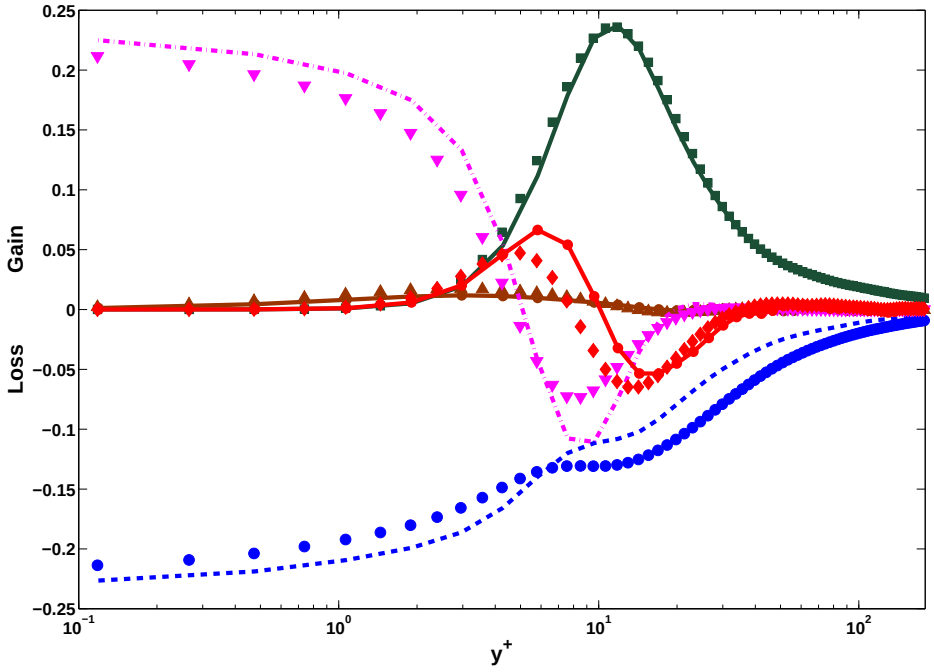

FIGURE 16. The turbulent-kinetic budget normalized by ν/u_τ^4 near the wall for $Re_\tau = 395$, compared with DNS by Moser *et al.* (1999). Production term: simplified model, solid line; DNS, square. Dissipation term: simplified model, dash-dash line; DNS, circle; Pressure transport term: simplified model, dash-dash line with circle; DNS, up-triangle. Viscous diffusion term: simplified model, dash-dot line; DNS, down-triangle. Turbulent convection term: simplified model, solid line with circle; DNS, diamond.

leads to

$$-\overline{u'v'} = l_m^2 \left|\frac{\mathrm{d}\bar{u}}{\mathrm{d}y}\right| \frac{\mathrm{d}\bar{u}}{\mathrm{d}y}. \tag{5.11}$$

The above model has been used extensively in the CFD softwares. Unfortunately, these assumptions are not really correct near the wall region. Thus, the Prandtl's mixing length theory cannot lead to any essential mechanism in the physics of turbulence. However, mixing length is still one of the most important length scales in turbulence, since it is regarded to be the size of the large eddies.

The variation of l_m with y^+ is shown in figure 17 for the simplified model. Near the wall, the mixing length displays a scaling of $l_m \sim {y^+}^{3/2}$ (She *et al.* 2010). Near the center of the flow, the scaling is $l_m \sim 1/\sqrt{1 - y^+/Re_\tau}$. This simplified model agrees well with the scaling in l_m near the wall and the center.

6. Summary and discussion

We present a new mathematical derivation of a closure relating the Reynolds stress to the mean strain rate for incompressible turbulent flows, based on the multiscale analysis of Navier-Stokes equation in three-dimensional space. Based on a systematic multiscale analysis and by using an iterative homogenization of the large and small scale solutions

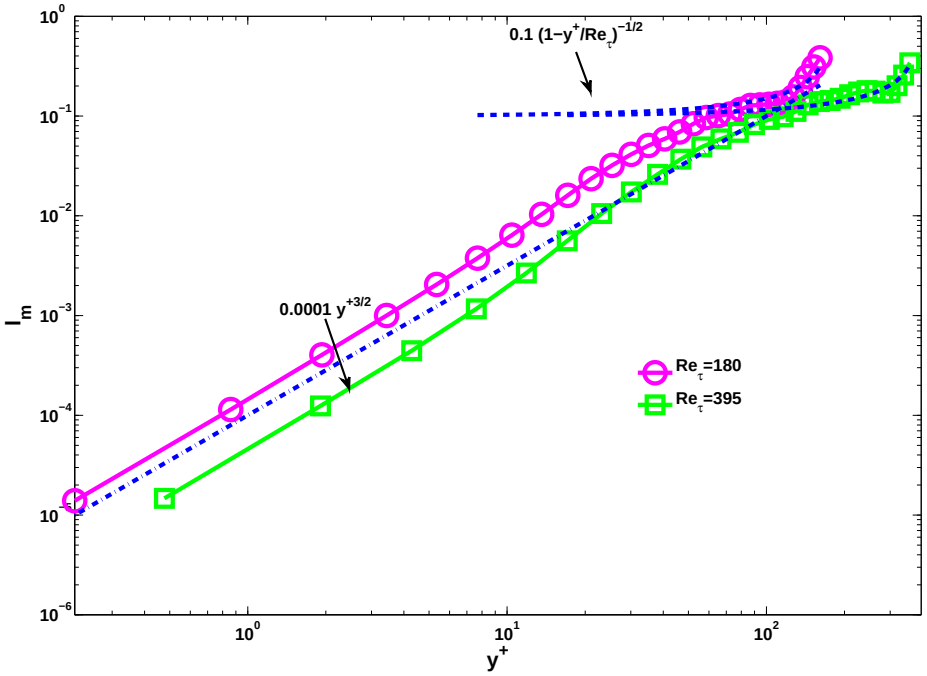

FIGURE 17. The mixing length for $\mathrm{Re}_\tau = 180$ and $\mathrm{Re}_\tau = 395$ by the simplified model.

dynamically, we identified a crucial structure of the Reynolds stress. As a consequence, we have established a linear constitutive relationship between the Reynolds stress and the strain rate for incompressible turbulent flows, up to second order accuracy of time step Δt. Further consideration of specific flows would enable us to produce an explicit formula for the Reynolds stress in two examples, homogeneous turbulence and turbulent channel flow. The Smagorinsky model has been recovered using this procedure of mathematical derivation for homogeneous turbulence. In addition, we have obtained a simplified Smagorinsky model for turbulence channel flow.

An extensive numerical study has been performed to validate the simplified model for turbulent channel flow, using some well-established benchmark tests and good agreement has been found with both experimental and DNS results. Currently, this procedure of mathematical derivation of turbulent models has been successfully applied to turbulent flow with a relatively simple geometry. It does shed light on the explanation of the physical mechanism by deriving a constitutive relationship between Reynolds stress and the strain rate through systematically mathematical analysis. Moreover, the analysis presented in this paper is quite general and can be applied to derive a leading order constitutive relation between the Reynolds stress and the strain rate for incompressible flows with different boundary geometries, and for other type of flows such as compressible and non-Newtonian flows.

Acknowledgments. This work was in part supported by the AFOSR MURI grant FA9550-09-1-0613. We would like to thank Professor Olivier Pironneau for many stimulating and inspiring discussions. His comments and suggestions have greatly improved

the quality of this work. We also thank Dr. Daniel Chung for providing the DNS code of turbulent channel flow.

Appendix A. Reparameterization of initial velocity in a two-scale structure

In this appendix, we would like to show how to reformulate any velocity $\boldsymbol{v}(x, y, z)$, which may contain infinitely many scales, in a two-scale structure. Assume $\boldsymbol{v}$ is periodic in x and z. The no-slip boundary condition is applied in y direction. Since this procedure can be done direction by direction, we can reparameterize in the periodic direction x and z and this has been shown in Hou *et al.* (2005, 2008). Thus, we only need to deal with the non-periodic direction y. The key idea is to use Sine transform, which not only has the same computational complexity of Fourier transform, but also incorporates the boundary condition.

Let $\boldsymbol{v}(x, y, z)$ be any function, which is periodic in (x, z) and zero on the boundaries in y, i.e. $\boldsymbol{v}(x, 0, z) = \boldsymbol{v}(x, 1, z) = 0$. Denoting $\boldsymbol{x} = (x, y, z)$ and $\boldsymbol{k} = (k_x, k_y, k_z)$, Fourier transform in x and z directions and sine transform in y direction read as

$$\boldsymbol{v}(x, y, z) = \sum_{\boldsymbol{k}=(k_x,k_y,k_z)} \hat{\boldsymbol{v}}_k \sin(\pi k_y y) \exp(2\pi i(k_x x + k_z z)).$$

Choose $0 < \epsilon = 1/E < 1$, where E is an integer, and let

$$\Lambda_E = \left\{ \boldsymbol{k}; |k_j| \leqslant \frac{E}{2}, j = (x, y, z) \right\}, \quad \Lambda'_E = Z^3 \backslash \Lambda_E. \tag{A 1}$$

Then by splitting into two parts in spectral space, the velocity can be rewritten as

$$\boldsymbol{v} = \boldsymbol{v}^{(l)}(\boldsymbol{x}) + \boldsymbol{v}^{(s)}(\boldsymbol{x}, \boldsymbol{x}/\epsilon), \tag{A 2}$$

where

$$\boldsymbol{z} = \boldsymbol{x}/\epsilon = (x/\epsilon, y/\epsilon, z/\epsilon)$$

The two terms in (A 2) are the large-scale velocity and the small-scale velocity respectively,

$$\boldsymbol{v}^{(l)}(\boldsymbol{x}) = \sum_{\boldsymbol{k}\in\Lambda_E} \hat{\boldsymbol{v}}(\boldsymbol{k}) \sin(\pi k_y y) \exp(2\pi i(k_x x + k_z z)),$$
$$\boldsymbol{v}^{(s)}(\boldsymbol{x}, \boldsymbol{y}) = \sum_{\boldsymbol{k}\in\Lambda'_E} \hat{\boldsymbol{v}}(\boldsymbol{k}) \sin(\pi k_y y) \exp(2\pi i(k_x x + k_z z)).$$

Rewrite each $\boldsymbol{k}$ in the following form

$$\boldsymbol{k} = E\boldsymbol{k}^{(s)} + \boldsymbol{k}^{(l)},$$

where

$$\boldsymbol{k}^{(s)} = (k_x^{(s)}, k_y^{(s)}, k_z^{(s)}), \quad \boldsymbol{k}^{(l)} = (k_x^{(l)}, k_y^{(l)}, k_z^{(l)}),$$

then we have

$$
\begin{aligned}
v^{(s)} &= \sum_{\boldsymbol{k}\in\Lambda'_E} \hat{\boldsymbol{v}}(\boldsymbol{k}) \sin(\pi k_y y) \exp(2\pi i(k_x x + k_z z)) \\
&= \sum_{E\boldsymbol{k}^{(s)}+\boldsymbol{k}^{(l)}\in\Lambda'_E} \hat{\boldsymbol{v}}(E\boldsymbol{k}^{(s)}+\boldsymbol{k}^{(l)}) \sin\left(\pi(Ek_y^{(s)}+k_y^{(l)})y\right) \exp\left(2\pi i((Ek_x^{(s)}+k_x^{(l)})x + (Ek_z^{(s)}+k_z^{(l)})z)\right) \\
&= \sum_{\boldsymbol{k}^{(s)}\neq 0} \left(\sum_{\boldsymbol{k}^{(l)}\in\Lambda_E} \hat{\boldsymbol{v}}(E\boldsymbol{k}^{(s)}+\boldsymbol{k}^{(l)}) \sin\left(\pi k_y^{(l)} y\right) \exp\left(2\pi i(k_x^{(l)}x + k_z^{(l)}z)\right)\right) \\
&\qquad \times \cos\left(\pi k_y^{(s)}(Ey)\right) \exp\left(2\pi i(k_x^{(s)}Ex + k_z^{(s)}Ez)\right) \\
&\quad + \sum_{\boldsymbol{k}^{(s)}\neq 0} \left(\sum_{\boldsymbol{k}^{(l)}\in\Lambda_E} \hat{\boldsymbol{v}}(E\boldsymbol{k}^{(s)}+\boldsymbol{k}^{(l)}) \cos\left(\pi k_y^{(l)} y\right) \exp\left(2\pi i(k_x^{(l)}x + k_z^{(l)}z)\right)\right) \\
&\qquad \times \sin\left(\pi k_y^{(s)}(Ey)\right) \exp\left(2\pi i(k_x^{(s)}Ex + k_z^{(s)}Ez)\right) \\
&= \sum_{\boldsymbol{k}^{(s)}\neq 0} \left(\hat{\boldsymbol{v}}_1(\boldsymbol{k}^{(s)},\boldsymbol{x}) \cos\left(\pi k_y^{(s)}(y/\epsilon)\right) + \hat{\boldsymbol{v}}_2(\boldsymbol{k}^{(s)},\boldsymbol{x}) \sin\left(\pi k_y^{(s)}(y/\epsilon)\right)\right) \exp\left(2\pi i(k_x^{(s)}x/\epsilon + k_z^{(s)}z/\epsilon)\right) \\
&= \boldsymbol{v}^{(s)}\left(\boldsymbol{x}, \frac{\boldsymbol{x}}{\epsilon}\right),
\end{aligned}
$$

where $\hat{\boldsymbol{v}}_1(\boldsymbol{k}^{(s)},\boldsymbol{x})$ and $\hat{\boldsymbol{v}}_2(\boldsymbol{k}^{(s)},\boldsymbol{x})$, which are in physical space, are the results of inverse transform of the large scale,

$$
\begin{aligned}
\hat{\boldsymbol{v}}_1(\boldsymbol{k}^{(s)},\boldsymbol{x}) &= \sum_{\boldsymbol{k}^{(l)}\in\Lambda_E} \hat{\boldsymbol{v}}(E\boldsymbol{k}^{(s)}+\boldsymbol{k}^{(l)}) \sin\left(\pi k_y^{(l)} y\right), \\
\hat{\boldsymbol{v}}_2(\boldsymbol{k}^{(s)},\boldsymbol{x}) &= \sum_{\boldsymbol{k}^{(l)}\in\Lambda_E} \hat{\boldsymbol{v}}(E\boldsymbol{k}^{(s)}+\boldsymbol{k}^{(l)}) \cos\left(\pi k_y^{(l)} y\right).
\end{aligned}
$$

Remark. Note that $v^{(s)}(\boldsymbol{x},\boldsymbol{z})$ is a periodic function in $\boldsymbol{z}$ with mean zero.

REFERENCES

Antonia, R. A., Teitel, M., Kim, J. & Browne, L. W. 1992 Low Reynolds number effects in a fully developed turbulent channel flow. *J. Fluid Mech.* **236**, 579–605.

Baggett, J. S. 1998 On the feasibility of merging les with rans for the near-wall region of attached turbulent flows. *Annual Research Briefs*, pp. 267-277. Center for Turbulence Research, NASA Ames/Stanford University.

Balint, Jean-Louis, Wallace, James M. & Vukoslavcevic, Petar 1991 The velocity and vorticity vector fields of a turbulent boundary layer. part 2. statistical properties. *J. Fluid Mech.* **228**, 53.

Berselli, L. C., Iliescu, T. & Layton, W. J. 2006 *Mathematics of Large Eddy Simulation of Turbulent Flows*. Springer.

Champagne, F. H., Friehe, C. A., LaRue, J. C. & Wyngaard, J. C. 1977 Flux measurements, flus extimation techniques and fine-scale turbulence measurements in the unstable surface layer over land. *J. Atmos. Sci* **34**, 515–530.

Chapman, D. R. 1979 Computational aerodynamics development and outlook. *AIAA Journal* **17**, 1293–1313.

Ciarlet, Philippe G. 1988 *Mathematical elasticity, Volume I: Three dimensional elasticity*. North-Holland, Elsevier Science Publisher.

van Driest, E. R. 1956 On turbulent flow near a wall. *J. Aerospace Sci* **23**, 1007–1011.

Eckelmann, H. 1974 The structure of the viscous sublayer and the adjacent wall region in a turbulent channel flow. *J. Fluid Mech.* **65**, 429–459.

Ferziger, J. H. 1977 Large eddy simulations of turbulent flows. *AIAA Journal* **15(9)**, 1261–1267.

Hamba, F. 2003 A hybrid rans/les simulation of turbulent channel flows. *Theoret. Comput. Fluid Dyn.* **16**, 387–403.

Hou, Thomas Y. & Li, Ruo 2007 Computing nearly singular solutions using pseudo-spectral methods. *J. Comp. Phys.* **226**, 379–397.

Hou, T. Y., Yang, D. P. & Ran, H. 2005 Multiscale analysis in Lagrangian formulation for the 2-D incompressible Euler equation. *Discrete and Continuous Dynamical System, Series A* **13**, 1153–1186.

Hou, T. Y., Yang, D. P. & Ran, H. 2008 Multiscale analysis and computation for the three-dimensional incompressible Navier-Stokes equations. *Multiscale Model. Simul.* **6**, 1317–1346.

Hussain, A. K. M. F. & Reynolds, W. C. 1970 The mechanics of an organized wave in turbulent shear flow. *J. Fluid Mech.* **41**, 241–258.

Jeong, Jinhee & Hussain, Fazle 1995 On the identification of a vortex. *J. Fluid Mech.* **285**, 69–94.

Jeong, J., Hussain, F., Schoppa, W. & Kim, J. 1997 Coherent structures near the wall in a turbulent channel flow. *J. Fluid Mech.* **332**, 185–214.

von Kármán, T. 1930 Mechanische Ahnlichkeit und turbulenz. In *Proc. Third Int. Congr. Applied Mechanics*, pp. 85–105. Stockholm.

Kastrinakis, E. G. & Eckelmann, H. 1983 Measurement of streamwise vorticity flucturations in a turbulent channel flow. *J. Fluid Mech.* **137**, 165–186.

Kim, J., Moin, P. & Moser, R. 1987 Turbulence Statisitics in Fully Developed Channel Flow at low Reynolds Number. *J. Fluid Mech.* **177**, 1317–1346.

Kreplin, H. & Eckelmann, H. 1979 Behavior of the three fluctuating velocity components in the wall region of a turbulent channel flow. *Phys. Fluids* **22** (7), 1233–1239.

Lamb, H. 1945 *Hydrodynamics*. Dover.

Lesieur, M. & Méais, O. 1996 New trends in large-eddy simulations of turbulence. *Ann. Rev. Fluid Mech.* **28**, 45–82.

Lilly, D. K. 1987 *Lecture notes on Turbulence*, pp. 171–218. World Scientific.

McLaughlin, D. W., Papanicolaou, G. C. & Pironneau, O. R. 1985 Convection of microstructure and related problems. *SIAM J. Appl. Math.* **45**, 780–797.

Moser, Robert D., Kim, John & Mansour, Nagi N. 1999 Direct numerical simulation of turbulent channel flow up to $re_\tau = 590$. *Phys. Fluids* **11** (4), 943–945.

Pope, S. B. 2000 *Turbulent Flows*. Cambridge university press.

Prandtl, L. 1925 Über die ausgebildete turbulenz. *Z. angew. Math. u. Mech* **5**, 136–139.

Rogallo, R. S. & Moin, P. 1984 Numerical simulation of turbulent flows. *Ann. Rev. Fluid Mech.* **16**, 99–137.

Sagaut, P. 2001 *Large eddy simulation for incompressible flows, an introduction*. Springer-Verlag.

Schoppa, W. & Hussain, F. 2002 Coherent structure generation in near-wall turbulence. *J. Fluid Mech.* **453**, 57–108.

She, Zhen-Su, Wu, You, Chen, Xi & Hussain, Fazle 2010 New perspective in statistical modeing of wall-bounded turbu. *Acta Mech. Sin* **26**, 847–861.

Smagorinsky, J. 1963 General circulation experiments with the primitive equations. i. the basic experiment. *Monthly Weather Review* **91**, 99–164.

Spalart, P., Moser, R & Rogers, M. 1994 Spectral Methods for the Navier-Stokes Equations with One Infinite and Two Periodic Directions. *J. Comp. Phys.* **96**, 297–324.

Spalart, P. R. 1988 Direct simulation of a turbulent boudnary layer up to $re_\theta = 1410$. *J. Fluid Mech.* **187**, 61–98.

Spalart, P. R., Jou, W. H., Strelets, M. & Allmaras, S. R. 1997 Comments on the feasibility of les for wings, and on a hybrid rans/les approach. In *First AFOSR International Conference on DNS/LES*, pp. 137–147.

Squires, K. D., Forsythe, J. R. & Spalart, P. R. 2005 Detached-eddy simulation of the separated flow over a rounded-corner square. *J. Fluids Eng.* **127**, 959–966.

Tennekes, H. & Lumley, J. L. 1972 *A first course in Turbulence*. MIT Press.

Willmarth, W. W. 1975 Pressure fluctuations beneath turbulent boundary layers. *Annual Review of Fluid Mechanics* **7** (1), 13–36.